
Dual-Resolution Correspondence Networks

Xinghui Li

Active Vision Lab

University of Oxford

xinghui@robots.ox.ac.uk

Kai Han

Visual Geometry Group

University of Oxford

khan@robots.ox.ac.uk

Shuda Li

Active Vision Lab

University of Oxford

shuda@robots.ox.ac.uk

Victor Adrian Prisacariu

Active Vision Lab

University of Oxford

victor@robots.ox.ac.uk

Abstract

We tackle the problem of establishing dense pixel-wise correspondences between a pair of images. In this work, we introduce Dual-Resolution Correspondence Networks (DRC-Net), to obtain pixel-wise correspondences in a coarse-to-fine manner. DRC-Net extracts both coarse- and fine- resolution feature maps. The coarse maps are used to produce a full but coarse 4D correlation tensor, which is then refined by a learnable neighbourhood consensus module. The fine-resolution feature maps are used to obtain the final dense correspondences guided by the refined coarse 4D correlation tensor. The selected coarse-resolution matching scores allow the fine-resolution features to focus only on a limited number of possible matches with high confidence. In this way, DRC-Net dramatically increases matching reliability and localisation accuracy, while avoiding to apply the expensive 4D convolution kernels on fine-resolution feature maps. We comprehensively evaluate our method on large-scale public benchmarks including HPatches, InLoc, and Aachen Day-Night. It achieves the state-of-the-art results on all of them.

1 Introduction

Establishing correspondences between a pair of images that shares a common field of view is critical for many important tasks in computer vision such as 3D reconstruction [1, 2, 3], camera motion estimation [4], relocalization [5, 6, 7, 8], etc. Most existing methods tackle the problem using a classic 3-stage pipeline, i.e., detection, description and matching [7, 9]. They first detect local repeatable salient points known as the keypoints, then describe these keypoints by extracting feature vectors from some local regions around them, and finally form the keypoint pairs, also known as the correspondences, by selecting a set of high confident matches from all possible candidate matches. The resulting correspondences can then be used to triangulate 3D coordinates for model reconstruction [1] or to feed the RANSAC Perspective-n-Point (PnP) algorithms [10, 11] for camera pose estimation [12, 13]. This pipeline has demonstrated great success in dealing with certain illumination or camera viewpoint variation using the classic hand-crafted local feature descriptors such as SIFT [14], SURF [15], BRISK [16] or the modern CNN features [17]. However, many of these methods are based on local support regions and therefore suffer from the missing detection problems [6]. During matching, they only consider up to k nearest neighbours, instead of the entire matching space, which also limits their performance especially under extreme appearance changes such as day-to-night with wide viewpoint variations.

Recently, several approaches [18, 19, 5] aim to avoid the detection stage by considering every point from a regular grid for matching. As a result, dense matches can be obtained by retrieving the

confident ones from all possible candidate matches. Hence, the missing detection problem can be alleviated. Among these approaches, the Neighbourhood Consensus Networks (NCNet) [5] and its variants [20, 21, 6] have shown encouraging results. These methods employ a CNN to extract features from two images, then calculate a 4D correlation tensor representing the entire matching space where each location records the cosine correlation score between a pair of feature vectors, and refine the correlation tensor by a sequence of 4D convolution kernels. The learnt 4D kernels turn out to be highly effective in filtering incorrect matches. However, the use of 4D convolution kernels in these methods are prohibitively expensive, restricting them from handling images with a high resolution or resulting in inadequate localisation accuracy.

In this paper, we propose Dual-Resolution Correspondence Networks (DRC-Net) to establish dense correspondences for high-resolution images in a coarse-to-fine manner. DRC-Net first extracts both coarse- and fine-resolution feature maps. Specifically, we employ an FPN-like [22] feature backbone to obtain the dual-resolution feature maps. Then, the coarse maps are used to produce a full 4D correlation tensor, which is then refined by the neighbourhood consensus module. The fine-resolution feature maps are used to obtain the final dense correspondences guided by the refined coarse 4D correlation tensor. Specifically, the full 4D tensor is used to select local regions in the high-resolution feature maps where the corresponding regions have high correlation scores, avoiding calculating the expensive full 4D correlation tensor for the high-resolution feature maps. When both the coarse and fine correlation scores are coupled together, a more reliable correspondences can be estimated from the candidate local regions for the high-resolution feature maps. This can drastically reduce the memory footprint and computation cost while boosting the matching results for more accurate localization.

The main contributions of this paper can be summarised as follow: First, we introduce a novel neural network architecture which generates dual-resolution feature maps allowing to match correspondences in a coarse-to-fine manner; second, the rough matches extracted from the coarse correlation tensor allow the model to focus on the local regions in the fine-resolution feature maps that are very likely to contain the correct matches. This dramatically reduces the memory footprint and computation cost for matching on fine-resolution feature maps; third, we comprehensively evaluate our method on large-scale public benchmarks including HPatches [23], InLoc [24], and Aachen Day-Night [13] achieving the state-of-the-art results on all of them, which demonstrates the effectiveness as well as generalisability of the proposed method. Our code will be made publicly available.

2 Related work

Establishing correspondences between two images has been investigated extensively for decades [25, 26, 19, 18], and it is the workhorse for many computer vision tasks such as 3D reconstruction, image retrieval, robot relocalization, etc. It is out of the scope of the paper to review all methods for correspondence estimation, and here we only review the most relevant ones.

The most popular approaches follow the 3-stage pipeline of detection, description and matching. Detecting salient and repeatable keypoints [27, 28, 29, 30, 7] allows a small memory and computation cost by the detected sparse 2D points, which can then be described using either hand-crafted feature descriptors [14, 15, 16, 31] or data-driven learning-based approaches [32, 33, 7, 8, 34, 35, 36, 37]. Finally, these keypoints with feature descriptors can then be paired together to form a candidate matching space from which a set of confident matches can be retrieved using random sampling schemes [38, 39] or validity check by inter-feature constraints [40, 3]. Although popular, the 3-stage pipeline suffers the missing detection problem [6]. In addition, each stage was trained separately, which brings extra complexity to deploy.

Recently, NCNet [5] was introduced to combine all the 3 stages into an end-to-end trainable framework while effectively incorporating the neighbourhood consensus constraint to filter outliers. In particular, NCNet first constructs a dense 4D matching tensor that contains all the possible matches in the feature space, and each element in the 4D matching tensor represents the matching score of one possible match. In this way, all possible pairs are considered, therefore, this could remedy the missing detection problem to some extent. NCNet then applies a sequence of 4D convolutions on the 4D matching tensor to realize the neighbour consensus constraint to refine the matching results. It has shown promising results for correspondence estimation. Inspired by NCNet, several methods have been proposed to improve this framework by using self-similarity to capture complex local pattern for

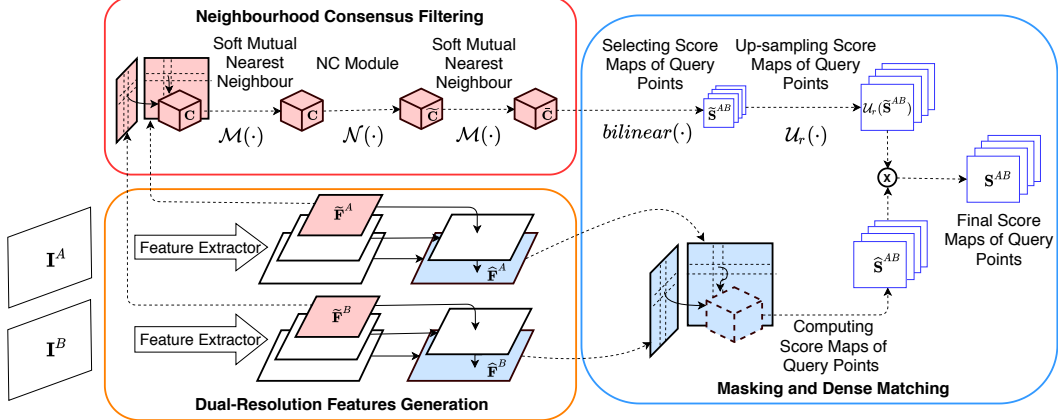


Figure 1: Overview of DRC-Net. The coarse feature map $\tilde{\mathbf{F}}^A$ and $\tilde{\mathbf{F}}^B$ (red) are combined to form the 4D correlation tensor \mathbf{C} which is then refined by the neighbourhood consensus module. The refined 4D tensor $\tilde{\mathbf{C}}$ can be used to generate the 2D score map $\tilde{\mathbf{S}}^{AB}$. After up-sampling $\tilde{\mathbf{S}}^{AB}$, it can be used to selected confident local regions in the fine-resolution feature maps $\hat{\mathbf{F}}^A$ and $\hat{\mathbf{F}}^B$ (blue) and to adjust the 2D correlation score map $\hat{\mathbf{S}}^{AB}$ from the fine-resolution feature maps to get the final correlation score map \mathbf{S}^{AB} , from which the dense correspondence can be retrieved. Best viewed in colour.

matching [20, 21] and introducing non-isotropic 4D filtering to better deal with scale variation [21]. One main drawback of NCNet is large memory consumption. The size of the 4D matching score tensor increases quadratically with the size of the images. Therefore, NCNet is not scalable to images with a high resolution. Very recently, we notice the concurrent pre-print work Sparse-NCNet [6] that tackles the problem by projecting the 4D correlation map into a 3D sub-manifold where ordinary convolution can be applied to achieve similar or better performance to NCNet. However, projecting the original 4D correlation to the sub-manifold might lose some useful information for matching. In contrast, our method maintains dual-resolution feature maps. We subtly use the coarse-resolution feature map to form a refined 4D matching tensor, which is used to adjust the matching score obtained using the fine-resolution features. In this way, our method can enjoy both the benefits of robust trainable neighbourhood consensus constraint and denser matching from the fine-resolution feature maps. As will be shown, our method can obtain better results than Sparse-NCNet using a smaller input image size.

Another series of relevant works are the CNN based methods for camera pose estimation [41, 42, 43, 44], where a pair of images are fed into a Siamese network [41, 42] to directly regress the relative pose. These methods are simple and effective, but typically applied to deal with small viewpoint changes and suffers limited capability of generalising to new scenes.

3 Method

We tackle the dense correspondence estimation problem by introducing the Dual-Resolution Correspondence Networks (DRC-Net) which establish correspondences in a coarse-to-fine manner. Figure 1 provides an overview of the DRC-Net. Specifically, we employ an FPN-like feature extractor to build both coarse- and fine-resolution feature maps. The coarse-resolution feature maps are then used to form the 4D correlation tensor which is then refined by the learnable neighbourhood consensus module. The refined 4D correlation tensor is then used to select local regions in the high-resolution feature maps where the corresponding regions in the refined 4D correlation tensor have high correlation scores. The final dense matches are then obtained by combining the local correlation maps from fine-resolution features with their corresponding 2D correlation maps generated from the refined 4D correlation tensor.

In the remainder of the section, we will first briefly describe the neighbourhood consensus module [35, 5, 20] in section 3.1, then describe our strategy to generate the dual-resolution feature maps in section 3.2, and then introduce our method using the dual-resolution feature maps for high accuracy dense correspondence estimation in section 3.3. The training loss is described in section 3.4.

3.1 Neighbourhood consensus filtering

The neighbourhood consensus using 4D convolutions was initially introduced in [5]. Given a pair of images \mathbf{I}^A and \mathbf{I}^B , their feature maps $\mathbf{F}^A \in \mathbb{R}^{C \times H_a \times W_a}$ and $\mathbf{F}^B \in \mathbb{R}^{C \times H_b \times W_b}$ can be extracted using a standard CNN feature backbone (e.g., VGG16 [45], ResNet [46]), where H and W are the height and width of the feature map and C is the number of channels. The complete matching space for all possible pair of locations can be represented by a 4D tensor $\mathbf{C} \in \mathbb{R}^{H_a \times W_a \times H_b \times W_b}$ with each element being the cosine correlation $\mathbf{C}_{ijkl} = \mathbf{f}_{ij}^{A\top} \mathbf{f}_{kl}^B / (\|\mathbf{f}_{ij}^A\|_2 \|\mathbf{f}_{kl}^B\|_2)$ where $\mathbf{f}_{ij}^I \in \mathbb{R}^C$ represents the feature vector at location (i, j) in \mathbf{F}^I , and $\|\cdot\|_2$ represents the L_2 norm. Essentially, \mathbf{C} contains all possible combinations of feature pairs in \mathbf{F}^A and \mathbf{F}^B . A local 4D neighbourhood in \mathbf{C} actually represents the matching consistency between two local regions from the images. If a match is correct, their neighbourhood consistency should be relatively high. Therefore, 4D convolutions can be applied to learn the consistency patterns from the training data. If we denote the 4D convolution layers as a function $\mathcal{N}(\cdot)$, the neighbourhood consensus filtering can be represented as $\tilde{\mathbf{C}} = \mathcal{N}(\mathbf{C}) + \mathcal{N}(\mathbf{C}^\top)^\top$ where \top denotes the matching direction swapping of two images, i.e., $\mathbf{C}_{ijkl}^\top = \mathbf{C}_{klij}$. This is to avoid the learning to be biased in one matching direction.

In addition, a cyclic matching constraint can be employed in the form of soft mutual nearest neighbour filter $\bar{\mathbf{C}} = \mathcal{M}(\tilde{\mathbf{C}})$ such that any resulting correlation score $\bar{\mathbf{C}}_{ijkl} \in \bar{\mathbf{C}}$ is high only if both $\tilde{\mathbf{C}}_{ijkl}$ and $\tilde{\mathbf{C}}_{klij}$ are high. Particularly, $\bar{\mathbf{C}}_{ijkl} = r_{ijkl}^A r_{ijkl}^B \tilde{\mathbf{C}}_{ijkl}$, where $r_{ijkl}^A = \tilde{\mathbf{C}}_{ijkl} / \max_{ab} \tilde{\mathbf{C}}_{abkl}$ and $r_{ijkl}^B = \tilde{\mathbf{C}}_{ijkl} / \max_{cd} \tilde{\mathbf{C}}_{ijcd}$. We apply the filtering before and after the neighbourhood consensus module following [5].

3.2 Dual-resolution feature map generation

It has been reported in the literature [5, 47, 6] that the resolution of the feature maps to constitute the 4D correlation tensor affects the accuracy. However, the high memory and computation cost of 4D tensors prevents most existing works from scaling to large feature maps. To avoid calculating the complete 4D tensor of the high-resolution feature maps, we propose to use the dual-resolution feature maps (see fig. 2), from which we can enjoy the benefits of both 4D convolutions based neighbourhood consensus on coarse-resolution feature maps and more reliable matching from the fine-resolution feature maps.

In particular, we adopt a FPN-like [22] feature backbone, which can extract a pair of interlocked coarse-resolution $\tilde{\mathbf{F}} \in \mathbb{R}^{h \times w}$ and fine-resolution feature map $\hat{\mathbf{F}} \in \mathbb{R}^{H \times W}$. The intuition of using FPN is that it fuses the contextual information from the top layers in the feature hierarchy into the bottom layers that mostly encode low-level information. In such way, the bottom layers can not only preserve their resolution but also contain rich high-level information, which makes them more robust for matching. Particularly, to maintain the high descriptiveness of the main feature backbone, we increase the number of output channels of the 1×1 conv kernels from 256 to that of the highest feature map (i.e. 1024). The aim is to increase the complexity of the descriptor and hence achieve higher accuracy during matching. The resolution for $\hat{\mathbf{F}}$ is 4 times of $\tilde{\mathbf{F}}$.

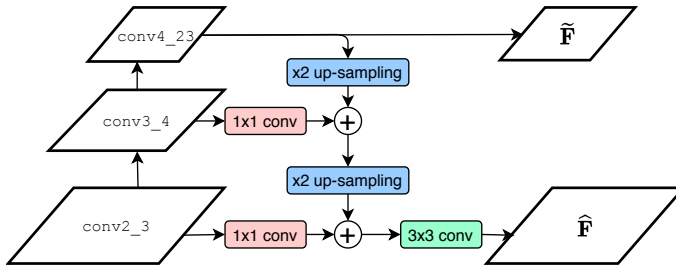


Figure 2: Dual-resolution feature map extractor. The fine-resolution feature map $\hat{\mathbf{F}}$ is 4 times larger than the coarse-resolution feature map $\tilde{\mathbf{F}}$, allowing denser, more reliable and better localised matches.

Such a dual-resolution structure allows us to establish a progressive matching pipeline. The coarse-resolution feature map $\tilde{\mathbf{F}}$ firstly produces 4D correlation tensor which is subsequently filtered by the

neighbourhood consensus module. The refined 4D score tensor is then used to identify and re-weight the local regions in the fine-resolution feature map $\widehat{\mathbf{F}}$, from which the final dense correspondences are obtained.

3.3 Masking and dense matching

Given a feature vector $\widehat{\mathbf{f}}_{ij}^A \in \widehat{\mathbf{F}}^A$, we compute its cosine correlation with all features in the target feature map $\widehat{\mathbf{F}}^B$ and generate a 2D score map $\widehat{\mathbf{S}}_{ij}^{AB} \in \mathbb{R}^{H_b \times W_b}$ by

$$\widehat{\mathbf{S}}_{ij,kl}^{AB} = \frac{\langle \mathbf{f}_{ij}^A, \mathbf{f}_{kl}^B \rangle}{\|\mathbf{f}_{ij}^A\|_2 \|\mathbf{f}_{kl}^B\|_2}, \quad \text{for all } k \in \{0, 1, \dots, H_b - 1\} \text{ and all } l \in \{0, 1, \dots, W_b - 1\}. \quad (1)$$

Let $r = \frac{H_a}{h_a} = \frac{W_a}{w_a}$ be the ratio between spatial dimensions of fine- and coarse-resolution feature maps, and (i', j') be the corresponding location of (i, j) on coarse-resolution feature map $\widetilde{\mathbf{F}}^A$. We have $\frac{i}{i'} = \frac{j}{j'} = r$. Notice that (i', j') may not be integers and hence we apply bilinear interpolation $\text{bilinear}(\cdot)$ to extract the 2D score map $\widetilde{\mathbf{S}}_{i'j'}^{AB}$ from $\widetilde{\mathbf{C}}$ by

$$\widetilde{\mathbf{S}}_{i'j',k'l'}^{AB} = \text{bilinear}(\widetilde{\mathbf{C}}_{\lceil i' \rceil \lceil j' \rceil k'l'}, \widetilde{\mathbf{C}}_{\lceil i' \rceil \lfloor j' \rfloor k'l'}, \widetilde{\mathbf{C}}_{\lfloor i' \rfloor \lceil j' \rceil k'l'}, \widetilde{\mathbf{C}}_{\lfloor i' \rfloor \lfloor j' \rfloor k'l'}), \quad (2)$$

where $\lceil \cdot \rceil$ and $\lfloor \cdot \rfloor$ denote the ceiling and floor of the input respectively and $\widetilde{\mathbf{S}}_{i'j'}^{AB} \in \mathbb{R}^{h_b \times w_b}$. This 2D score map $\widetilde{\mathbf{S}}_{i'j'}^{AB}$ will then serve as a “mask” to adjust the fine-resolution score map $\widehat{\mathbf{S}}_{ij}^{AB}$. For each score on $\widetilde{\mathbf{S}}_{i'j'}^{AB}$, it corresponds to an $r \times r$ region on $\widehat{\mathbf{S}}_{ij}^{AB}$. Hence we up-sample $\widetilde{\mathbf{S}}_{i'j'}^{AB}$ by r times to the same size as $\widehat{\mathbf{S}}_{ij}^{AB}$ using nearest neighbour. Let $\mathcal{U}_r(\cdot)$ be this up-sampling operation, we can then use $\widetilde{\mathbf{S}}_{i'j'}^{AB}$ to mask over $\widehat{\mathbf{S}}_{ij}^{AB}$ to produce the final score map \mathbf{S}_{ij}^{AB} by

$$\mathbf{S}_{ij}^{AB} = \widehat{\mathbf{S}}_{ij}^{AB} \odot \mathcal{U}_r(\widetilde{\mathbf{S}}_{i'j'}^{AB}), \quad (3)$$

where \odot represents the element-wise multiplication between two matrices.

For point (i, j) of in $\widehat{\mathbf{F}}^A$, its correspondence in $\widehat{\mathbf{F}}^B$ is then retrieved by $(k^*, l^*) = \text{argmax}_{kl} \mathbf{S}_{ij,kl}^{AB}$. By querying all (i, j) on $\widehat{\mathbf{F}}^A$, we can obtain a set of dense matches $\{(i_n, j_n), (k_n, l_n)\}_{n=1}^N$. In order to filter the outliers, we adopt the mutual nearest neighbour criteria. Namely, we obtain the dense match sets from both $\widehat{\mathbf{F}}^A$ to $\widehat{\mathbf{F}}^B$ and $\widehat{\mathbf{F}}^B$ to $\widehat{\mathbf{F}}^A$, and only keep the intersection of two sets as our final set of matches. However, exhaustively querying all features from the fine-resolution feature map is time-consuming. Hence, we adopt a simple strategy to speed up the matching procedure. Firstly, we establish a set of matches for all features in coarse feature map $\widetilde{\mathbf{F}}^A$, denoted as $\{(i'_n, j'_n), (k'_n, l'_n)\}_{n=1}^M$, which can be directly retrieved from $\widetilde{\mathbf{C}}$. We then sort scores of these matches in descending order and select top 50% of them. As each spatial location on $\widetilde{\mathbf{F}}^A$ corresponds to an $r \times r$ region in $\widehat{\mathbf{F}}^A$, we query all features in $\widehat{\mathbf{F}}^A$ that lie in the corresponding local region of top 50% of $\{(i'_n, j'_n)\}_{n=1}^M$ and apply the mutual neighbour criteria as described above. This effectively reduces the number of queries by half and increases speed.

3.4 Training loss

Due to the absence of dense keypoint annotations, existing methods normally use either image-level pairwise annotations [5, 20, 6] or sparse keypoint annotations [21] for training. We follow [21] to adopt the training loss based on sparse keypoint annotations. Specifically, the loss is defined as

$$\mathcal{L} = \|\mathbf{S}^{AB} - \mathbf{S}_{gt}^{AB}\|_F + \|\mathbf{S}^{BA} - \mathbf{S}_{gt}^{BA}\|_F, \quad (4)$$

where $\mathbf{S}^{AB} \in \mathbb{R}^{N \times T}$ is the probability map given N query keypoints in the source image w.r.t. the whole frame of the target feature map $\widehat{\mathbf{F}}^B$. $T = H_b \times W_b$ is the total number of elements in the fine-resolution feature map. \mathbf{S}_{gt}^{AB} is the ground truth. $\|\cdot\|_F$ is the Frobenius norm. To provide smoother learning signal from the ground truth, we follow [21] to apply the Gaussian blurring on \mathbf{S}_{gt}^{AB} and \mathbf{S}_{gt}^{BA} .

4 Experimental results

We evaluate our model on three challenging public datasets, HPatches [23], InLoc [24] and Aachen Day-Night [48] that contain huge viewpoint and illumination variations of both indoor and outdoor scenes. Our method substantially outperforms state-of-the-art methods. Our code and models will be made publicly available.

Implementation details We implemented our pipeline in Pytorch [49]. For feature extractor, we use ResNet101 pre-trained on ImageNet and truncate the part after conv4_23. It is fixed during training. For fine-resolution feature maps, we extract the output of conv2_3, conv3_4 and fuse the output of conv4_23 and conv3_4 into the output of conv2_3 in the way depicted in Figure 2. The 1×1 conv layers and the 3×3 conv fusing layers are fine-tuned. Comparison on different variants of the dual-resolution feature backbone can be find in Appendix A. For the neighbourhood consensus module, we use the same configuration as [5]. We train our model using Adam optimizer [50] for 15 epochs with an initial learning rate of 0.01 which is halved every 5 epochs.

Training data Following [7], we train our models on MegaDepth dataset [51], which consists of a large number of internet images about 196 scenes and their sparse 3D point clouds are constructed by COLMAP [52, 53]. The camera intrinsic and extrinsic together with the depth maps of 102, 681 are also included. We also follow [7] to generate sparse ground truth labels. First, we compare the overlap in sparse SfM point cloud between all image pairs to select the pairs whose overlap is over 50%. Next, for all selected pairs, the second image with depth information is projected into the first image and occlusion is removed by depth check. Then, we randomly collect 128 correspondences from each image pair to train our model. We use the scenes with more than 500 valid image pairs for training and the rest scenes for validation. To avoid scene bias, 110 image pairs are randomly selected from each training scene to constitute our training set. In total, we obtain 15, 070 training pairs and 14, 638 validation pairs. After training, we evaluate our model on HPatches, InLoc and Aachen Day-Night to validate the effectiveness and generalisability.

4.1 HPatches

HPatches benchmark [23] contains homography patches under significant illumination and viewpoint change. We follow the evaluation protocol of [6], where 108 image sequences are evaluated, with 56 of them about viewpoint change and 52 of them about illumination change. Each sequence consists of one reference image and five query images. Each query image pairs with one reference image hence five image pairs are obtained for each sequence. Homography w.r.t. to the reference image is provided for each query image. For each image pairs, matches in query image are projected into reference image using homography provided. We adopt the commonly used Mean Matching Accuracy (MMA) as evaluation metric

$$\text{MMA}(\{\mathbf{p}_i^A, \mathbf{p}_i^B\}_{i=1}^N; t) = \frac{\sum_{i=1}^N \mathbb{1}(t - \|H(\mathbf{p}_i^A) - \mathbf{p}_i^B\|_2)}{N}, \quad (5)$$

where t is the threshold of 2D distance. $\mathbb{1}(\cdot)$ is a binary indicator function whose output is 1 for non-negative value and 0 otherwise. $H(\cdot)$ denotes the warping by homography.

DRC-Net vs other neighbourhood consensus methods In Figure 12, we compare our approach with two neighbourhood consensus based methods, namely the NCNet [5] baseline, and the very recent pre-print Sparse-NCNet [6] which shows the state-of-the-art result. As can be seen, our method outperforms both Sparse-NCNet and NCNet by a significant margin under illumination change. In general, our method performs on par with Sparse-NCNet under viewpoint change. Sparse-NCNet slightly outperforms our method with a threshold smaller than 6 pixels, while our method outperforms Sparse-NCNet with a threshold larger than 6 pixels. Overall, our method notably outperforms both competitor methods. The feature map resolution is the key for robust matching. To have the feature map with a resolution of 200×150 , NCNet needs to take an image with a resolution of 3200×2400 . Sparse-NCNet can obtain a feature map resolution of 400×300 with the same input image size by reducing the stride of the last convolution layer in the feature extractor. In contrast, our method can obtain a feature map with the resolution of 400×300 by only using the input image with a resolution of 1600×1200 . Please refer to Appendix B for more comparison. Figure 4 demonstrates the qualitative results of two image pairs. More qualitative results can be found in Appendix C.

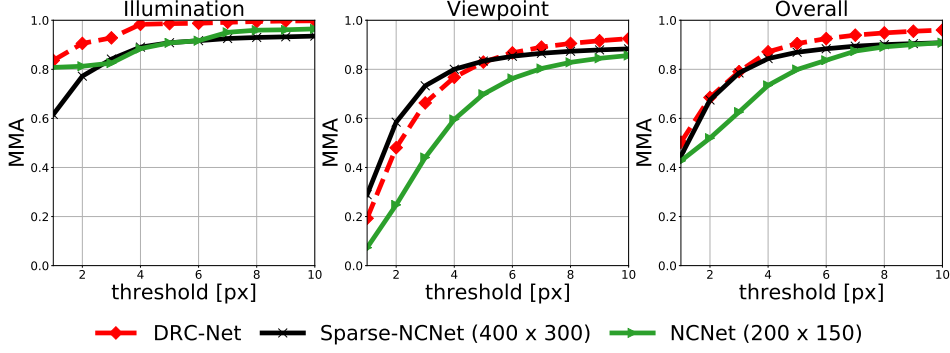


Figure 3: DRC-Net vs other neighbourhood consensus methods on HPatches. For each method, top 2000 matches are selected for evaluation.



Figure 4: Qualitative results on HPatches. Top 2000 matches are selected with $t = 3$ pixels. Our method is robust to huge viewpoint (left pair) and illumination (right pair) changes. Green and red dots denote correct and incorrect matches respectively (best viewed in PDF with zoom).

DRC-Net vs other state-of-the-art methods In Figure 5, we compare our method with DEFL [54], R2D2 [8], SuperPoint [33] and D2-Net [7]. The general trend is similar to the comparison with NCNet and Sparse-NCNet. Overall, DRC-Net substantially outperforms all other methods.

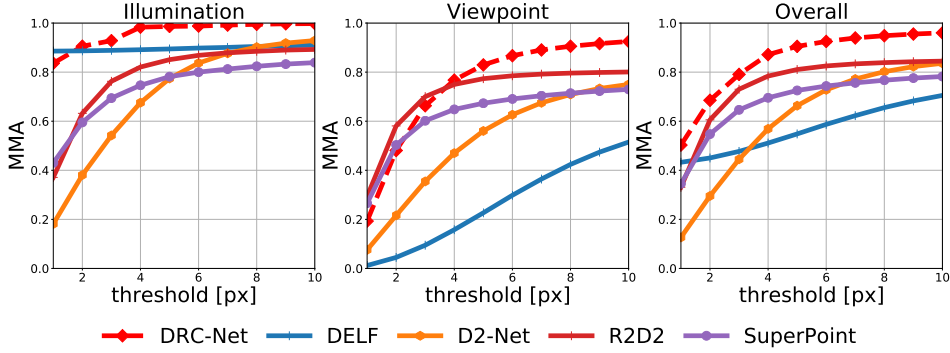


Figure 5: DRC-Net vs other state-of-the-art methods on HPatches. For other methods, top 2000 feature points are selected. By enforcing mutual nearest neighbour, they roughly generate 1000 matches for each image pairs. Hence we select top 1000 matches for fair comparison.

4.2 InLoc

InLoc benchmark [24] is designed to test the performance on long-term indoor relocalization. It consists of a large collection of images with depth acquired by the 3D scanner. Query images are taken by a smartphone camera a few months later. The benchmark contains very challenging viewpoint and illumination changes. We follow the evaluation protocol in [24]. For each query image, 10 candidate database images are selected. DRC-Net then establishes the correspondence between each pairs. Finally PnP solver is used to estimate the pose of the query image. The result is shown in Figure 6. We achieve the state-of-the-art result with distance threshold $> 0.3\text{m}$ and outperform the second best method by a significant margin. More qualitative results can be found in Appendix C.

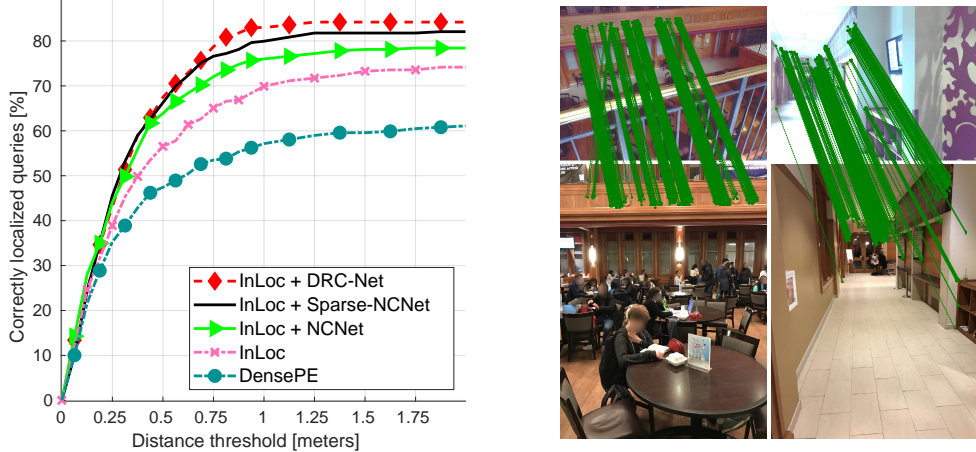


Figure 6: Evaluation on InLoc benchmark. Left: The result on InLoc benchmark. Right: Qualitative results of top 500 matches (best viewed in PDF with zoom). It is clear that our model is able to generate reliable correspondences under large viewpoint and illumination change.

4.3 Aachen Day-Night

Aachen Day-Night benchmark [48] is adopted to validate the performance on outdoor relocalization under illumination change. It has 98 night query images and each of them has 20 day-time candidate database images. We use DRC-Net to establish the correspondences for pose estimation. The result is presented in Figure 7. Our method achieves the state-of-the-art result for threshold (1m, 5°) and (5m, 10°). The result for (0.5m, 2°) is on par with the state-of-the-art. More qualitative results can be found in Appendix C.

Method	Correctly localized queries (%)		
	0.5m, 2°	1m, 5°	5m, 10°
RootSIFT [55]	36.1	54.1	72.5
DELF [54]	38.8	62.2	85.7
SuperPoint [33]	42.8	57.1	75.5
D2-Net [7]	44.9	66.3	88.8
R2D2 (N=8) [8]	45.9	66.3	88.8
Sparse-NCNet [6]	44.9	68.4	86.7
DRC-Net	44.9	68.4	88.8

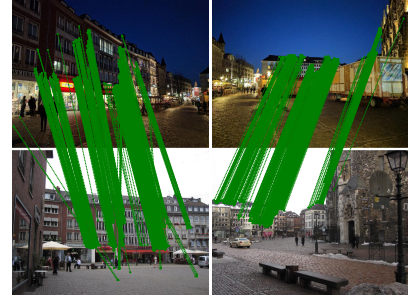


Figure 7: Evaluation on Aachen Day-Night benchmark. Left: Comparison with other methods. Right: Qualitative results of top 500 matches (best viewed in PDF with zoom). As demonstrated, DRC-Net achieves accurate matching under day-night and viewpoint change.

5 Conclusion

We have presented an end-to-end dual-resolution architecture, called DRC-Net, that can establish dense pixel-wise correspondences between a pair of images in a coarse-to-fine manner. DRC-Net first obtains a full 4D correlation tensor from the coarse-resolution feature maps, which is refined by the learnable neighbourhood consensus module. The refined correlation tensor is then used to guide the model to obtain robust matching from fine-resolution feature maps. In this way, DRC-Net dramatically increases matching reliability and localisation accuracy, while avoiding to apply the expensive 4D convolution kernels on fine-resolution feature maps. We comprehensively evaluate our method on large-scale public benchmarks HPatches, InLoc and Aachen Day-Night, achieving the state-of-the-art results.

Broader Impact

The proposed model enjoys great potential to improve a wide range of industrial applications including image alignment and retrieval, vision-based 3D reconstruction and camera pose localisation, etc. Particularly, the proposed method sets a new record of accuracy on both indoor and outdoor relocalization benchmarks which strongly indicates that it will directly benefit many fields in the near future including robotics, autonomous driving and gaming industry, where the vision-based relocalisation is the foundation. It is particularly important if the application has to work in a GPS-denied environment. Furthermore, with the potential of being able to deploy on mobile platforms such as robots, drones, smartphone, head-mounted display, the proposed method could be used to boost mixed/virtual reality for entertainment or education. It may be applied to build large-scale long-term indoor/outdoor maps which allows pinpointing a user’s location without GPS using images. This may also improve existing navigation capability of robots or drones and enable a more intelligent agent for various tasks such as delivery, searching and rescue.

In the meanwhile, the proposed model, like many other machine learning technology, does have some unwelcomed repercussions. The accurate and robust vision-only correspondence estimation and the subsequent localisation can be used to illegally locate a person or property without permission using an image circulated online. It may even be weaponized to guide a UAV to carry out a terrorism attack. However, these negative impacts are more related to the fields of application rather than the technology itself. Generally, proper legislation may be required to prevent any machine learning method from being used for evil purposes. Fortunately, many countries have already started to debate and evaluate the pros and cons of specific AI technology. For example, some countries have banned using facial recognition or restrict employing AI for surveillance. Therefore, we believe, under strict supervision, that our work will bring more benefits than harms to society.

Acknowledgments

We gratefully acknowledge the support of the European Commission Project Multiple-actOrs Virtual EmpathicCARegiver for the Elder (MoveCare) and the EPSRC Programme Grant Seebibyte EP/M013774/1. We are also grateful for the generous help of Mr. Mihai Dusmanu and Mr. Ignacio Rocco on certain technical issues.

References

- [1] Johannes L. Schönberger and Jan-Michael Frahm. Structure-from-motion revisited. In *Proceedings of IEEE Intl. Conf. on Computer Vision and Pattern Recognition (CVPR)*, 2016.
- [2] Runze Zhang. Distributed very large scale bundle adjustment by global camera consensus. In *Proceedings of Intl. Conf. on Computer Vision (ICCV)*, 2017.
- [3] Jiahui Zhang, Dawei Sun, Zixin Luo, Anbang Yao, Lei Zhou, Tianwei Shen, Yurong Chen, Hongen Liao, and Long Quan. Learning two-view correspondences and geometry using order-aware network. In *Proceedings of Intl. Conf. on Computer Vision (ICCV)*, 2019.
- [4] Shiwei Li, Lu Yuan, Jian Sun, and Long Quan. Dual-feature warping-based motion model estimation. In *Proceedings of Intl. Conf. on Computer Vision (ICCV)*, 2015.
- [5] Ignacio Rocco, Mircea Cimpoi, Relja Arandjelović, Akihiko Torii, Tomas Pajdla, and Josef Sivic. Neighbourhood consensus networks. In *Proceedings of Conf. on Neural Information Processing Systems (NeurIPS)*, 2018.
- [6] Ignacio Rocco, Relja Arandjelović, and Josef Sivic. Efficient neighbourhood consensus networks via submanifold sparse convolutions. In *arXiv preprint*, 2020.
- [7] Mihai Dusmanu, Ignacio Rocco, Tomas Pajdla, Marc Pollefeys, Josef Sivic, Akihiko Torii, and Torsten Sattler. D2-net: A trainable cnn for joint detection and description of local features. In *Proceedings of IEEE Intl. Conf. on Computer Vision and Pattern Recognition (CVPR)*, 2019.
- [8] Jerome Revaud, Philippe Weinzaepfel, César De Souza, Noe Pion, Gabriela Csurka, Yohann Cabon, and Martin Humenberger. R2D2: Repeatable and Reliable Detector and Descriptor. In *Proceedings of Conf. on Neural Information Processing Systems (NeurIPS)*, 2019.

- [9] Zixin Luo, Lei Zhou, Xuyang Bai, Hongkai Chen, Jiahui Zhang, Yao Yao, Shiwei Li, Tian Fang, and Long Quan. Aslfeat: Learning local features of accurate shape and localization. In *Proceedings of IEEE Intl. Conf. on Computer Vision and Pattern Recognition (CVPR)*, 2020.
- [10] Joel A. Hesch and Stergios I. Roumeliotis. A direct least-squares (dls) method for pnp. In *Proceedings of Intl. Conf. on Computer Vision (ICCV)*, 2011.
- [11] Tong Ke and Stergios Roumeliotis. An efficient algebraic solution to the perspective-three-point problem. In *Proceedings of IEEE Intl. Conf. on Computer Vision and Pattern Recognition (CVPR)*, 2017.
- [12] Shuda Li and Andrew Calway. Absolute pose estimation using multiple forms of correspondences from rgb-d frames. In *Proceedings of IEEE Intl. Conf. on Robotics and Automation (ICRA)*, 2016.
- [13] Torsten Sattler, Akihiko Torii, Josef Sivic, Marc Pollefeys, Hajime Taira, Masatoshi Okutomi, and Tomas Pajdla. Are large-scale 3d models really necessary for accurate visual localization? In *Proceedings of IEEE Intl. Conf. on Computer Vision and Pattern Recognition (CVPR)*, 2017.
- [14] David G Lowe. Distinctive image features from scale-invariant keypoints. *Intl. Journal of Computer Vision (IJCV)*, 2004.
- [15] Herbert Bay, Tinne Tuytelaars, and Luc Van Gool. Surf: Speeded up robust features. In *Proceedings of the European Conference on Computer Vision (ECCV)*, 2006.
- [16] Stefan Leutenegger, Margarita Chli, and Roland Y Siegwart. Brisk: Binary robust invariant scalable keypoints. In *Proceedings of Intl. Conf. on Computer Vision (ICCV)*, 2011.
- [17] Tsun Yi Yang, Jo Han Hsu, Yen Yu Lin, and Yung Yu Chuang. Deepcd: Learning deep complementary descriptors for patch representations. In *Proceedings of Intl. Conf. on Computer Vision (ICCV)*, 2017.
- [18] Xi Shen, François Fleuret, Alexei A. Efros, and Mathieu Aubry. Ransac-flow: generic two-stage image alignment. In *arXiv preprint*, 2020.
- [19] Ce Liu, Jenny Yuen, and Antonio Torralba. Sift flow: Dense correspondence across scenes and its applications. *IEEE Trans. Pattern Anal. Machine Intell. (PAMI)*, 2011.
- [20] Shuaiyi Huang, Qiuyue Wang, Songyang Zhang, Shipeng Yan, and Xuming He. Dynamic context correspondence network for semantic alignment. In *Proceedings of Intl. Conf. on Computer Vision (ICCV)*, 2019.
- [21] Shuda Li, Kai Han, Theo W. Costain, Henry Howard-Jenkins, and Victor Prisacariu. Correspondence networks with adaptive neighbourhood consensus. In *Proceedings of IEEE Intl. Conf. on Computer Vision and Pattern Recognition (CVPR)*, 2020.
- [22] Tsung-yi Lin, Piotr Dollár, Ross Girshick, Kaiming He, Bharath Hariharan, Serge Belongie, and Facebook AI. Feature pyramid networks for object detection. In *Proceedings of IEEE Intl. Conf. on Computer Vision and Pattern Recognition (CVPR)*, 2017.
- [23] Vassileios Balntas, Karel Lenc, Andrea Vedaldi, and Krystian Mikolajczyk. Hpatches: A benchmark and evaluation of handcrafted and learned local descriptors. In *Proceedings of IEEE Intl. Conf. on Computer Vision and Pattern Recognition (CVPR)*, 2017.
- [24] Hajime Taira, Masatoshi Okutomi, Torsten Sattler, Mircea Cimpoi, Marc Pollefeys, Josef Sivic, Tomas Pajdla, and Akihiko Torii. InLoc: Indoor visual localization with dense matching and view synthesis. In *Proceedings of IEEE Intl. Conf. on Computer Vision and Pattern Recognition (CVPR)*, 2018.
- [25] Relja Arandjelovic, Petr Gronat, Akihiko Torii, Tomas Pajdla, and Josef Sivic. Netvlad: Cnn architecture for weakly supervised place recognition. In *Proceedings of IEEE Intl. Conf. on Computer Vision and Pattern Recognition (CVPR)*, 2016.
- [26] Mikaela Angelina, Uy Gim, and Hee Lee. Pointnetvlad : Deep point cloud based retrieval for large-scale place recognition supplementary material. In *Proceedings of IEEE Intl. Conf. on Computer Vision and Pattern Recognition (CVPR)*, 2018.
- [27] Edward Rosten, Reid Porter, and Tom Drummond. Faster and better: a machine learning approach to corner detection. *IEEE Trans. Pattern Anal. Machine Intell. (PAMI)*, 2010.
- [28] Steffen Gauglitz, Tobias Höllerer, and Matthew Turk. Evaluation of interest point detectors and feature descriptors for visual tracking. *Intl. Journal of Computer Vision (IJCV)*, 2011.

- [29] Titus Cieslewski, Michael Bloesch, and Davide Scaramuzza. Matching features without descriptors: Implicitly matched interest points (imips). In *Proceedings of British Machine Vision Conference (BMVC)*, 2019.
- [30] Axel Barroso-laguna, Edgar Riba, and Daniel Ponsa. Key.net : Keypoint detection by handcrafted and learned cnn filters formulas formulas motivation : Handcrafted features. In *Proceedings of Int'l. Conf. on Computer Vision (ICCV)*, 2019.
- [31] Johannes Lutz Schönberger, Hans Hardmeier, Torsten Sattler, and Marc Pollefeys. Comparative evaluation of hand-crafted and learned local features comparative evaluation of hand-crafted and learned local features. In *Proceedings of IEEE Int'l. Conf. on Computer Vision and Pattern Recognition (CVPR)*, 2017.
- [32] Yurun Tian, Xin Yu, Bin Fan, Fuchao Wu, Huub Heijnen, and Vassileios Balntas. Sosnet: Second order similarity regularization for local descriptor learning. In *Proceedings of IEEE Int'l. Conf. on Computer Vision and Pattern Recognition (CVPR)*, 2019.
- [33] Daniel DeTone, Tomasz Malisiewicz, and Andrew Rabinovich. Superpoint: Self-supervised interest point detection and description. In *Proceedings of IEEE Int'l. Conf. on Computer Vision and Pattern Recognition (CVPR)*, 2018.
- [34] Aritra Bhowmik, Stefan Gumhold, Carsten Rother, and Eric Brachmann. Reinforced feature points: Optimizing feature detection and description for a high-level task. In *Proceedings of IEEE Int'l. Conf. on Computer Vision and Pattern Recognition (CVPR)*, 2020.
- [35] Jia Wang Bian, Wen Yan Lin, Yun Liu, Le Zhang, Sai Kit Yeung, Ming Ming Cheng, and Ian Reid. GMS: Grid-Based Motion Statistics for Fast, Ultra-robust Feature Correspondence. In *Proceedings of IEEE Int'l. Conf. on Computer Vision and Pattern Recognition (CVPR)*, 2019.
- [36] Kai Han, Rafael S. Rezende, Bumsuk Ham, Kwan-Yee K. Wong, Minsu Cho, Cordelia Schmid, and Jean Ponce. Scnet: Learning semantic correspondence. In *Proceedings of Int'l. Conf. on Computer Vision (ICCV)*, 2017.
- [37] Junghyup Lee, Dohyung Kim, Jean Ponce, and Bumsuk Ham. Sfnet: Learning object-aware semantic correspondence. In *Proceedings of IEEE Int'l. Conf. on Computer Vision and Pattern Recognition (CVPR)*, 2019.
- [38] Ondrej Chum and Jiri Matas. Matching with prosac – progressive sample consensus. In *Proceedings of IEEE Int'l. Conf. on Computer Vision and Pattern Recognition (CVPR)*, 2005.
- [39] Rahul Raguram, Ondrej Chum, Marc Pollefeys, Jiri Matas, and Jan Michael Frahm. USAC: A universal framework for random sample consensus. *IEEE Trans. Pattern Anal. Machine Intell. (PAMI)*, 2013.
- [40] Paul-Edouard Sarlin, Daniel DeTone, Tomasz Malisiewicz, and Andrew Rabinovich. Superglue: Learning feature matching with graph neural networks. In *Proceedings of IEEE Int'l. Conf. on Computer Vision and Pattern Recognition (CVPR)*, 2020.
- [41] Iaroslav Melekhov, Juha Ylioinas, Juho Kannala, and Esa Rahtu. Relative camera pose estimation using convolutional neural networks. In *arXiv preprint*, 2017.
- [42] Zakaria Laskar, Iaroslav Melekhov, Surya Kalia, and Juho Kannala. Camera relocalization by computing pairwise relative poses using convolutional neural network. *Proceedings of Int'l. Conf. on Computer Vision Workshops (ICCVW)*, 2018.
- [43] Vassileios Balntas, Shuda Li, and Victor Prisacariu. Relocnet: Continuous metric learning relocalisation using neural nets. In *Proceedings of the European Conference on Computer Vision (ECCV)*, 2018.
- [44] Mingyu Ding, Zhe Wang, Jiankai Sun, Jianping Shi, and Ping Luo. Camnet: Coarse-to-fine retrieval for camera re-localization. In *Proceedings of Int'l. Conf. on Computer Vision (ICCV)*, 19.
- [45] Karen Simonyan and Andrew Zisserman. Very deep convolutional networks for large-scale image recognition. In *Proceedings of Int'l. Conf. on Learning Representations (ICLR)*, 2015.
- [46] Kaiming He, Xiangyu Zhang, Shaoqing Ren, and Jian Sun. Deep residual learning for image recognition. In *Proceedings of IEEE Int'l. Conf. on Computer Vision and Pattern Recognition (CVPR)*, 2016.
- [47] Juhong Min, Jongmin Lee, Jean Ponce, and Minsu Cho. Hyperpixel flow: Semantic correspondence with multi-layer neural features. In *Proceedings of Int'l. Conf. on Computer Vision (ICCV)*, 2019.

- [48] Torsten Sattler, Will Maddern, Carl Toft, Akihiko Torii, Lars Hammarstrand, Erik Stenborg, Daniel Safari, Masatoshi Okutomi, Marc Pollefeys, Josef Sivic, Fredrik Kahl, and Tomas Pajdla. Benchmarking 6dof outdoor visual localization in changing conditions. In *Proceedings of IEEE Intl. Conf. on Computer Vision and Pattern Recognition (CVPR)*, 2018.
- [49] Adam Paszke, Sam Gross, Francisco Massa, Adam Lerer, James Bradbury, Gregory Chanan, Trevor Killeen, Zeming Lin, Natalia Gimelshein, Luca Antiga, Alban Desmaison, Andreas Kopf, Edward Yang, Zachary DeVito, Martin Raison, Alykhan Tejani, Sasank Chilamkurthy, Benoit Steiner, Lu Fang, Junjie Bai, and Soumith Chintala. Pytorch: An imperative style, high-performance deep learning library. In *Proceedings of Conf. on Neural Information Processing Systems (NeurIPS)*. 2019.
- [50] Diederik P. Kingma and Jimmy Ba. Adam: A method for stochastic optimization. In *Proceedings of Intl. Conf. on Learning Representations (ICLR)*, 2015.
- [51] Zhengqi Li and Noah Snavely. Megadepth: Learning single-view depth prediction from internet photos. In *Proceedings of IEEE Intl. Conf. on Computer Vision and Pattern Recognition (CVPR)*, 2018.
- [52] Johannes Lutz Schönberger and Jan-Michael Frahm. Structure-from-motion revisited. In *Proceedings of IEEE Intl. Conf. on Computer Vision and Pattern Recognition (CVPR)*, 2016.
- [53] Johannes Lutz Schönberger, Enliang Zheng, Marc Pollefeys, and Jan-Michael Frahm. Pixelwise view selection for unstructured multi-view stereo. In *Proceedings of the European Conference on Computer Vision (ECCV)*, 2016.
- [54] Hyeonwoo Noh, Andre Araujo, Jack Sim, Tobias Weyand, and Bohyung Han. Large-scale image retrieval with attentive deep local features. In *Proceedings of Intl. Conf. on Computer Vision (ICCV)*, 2017.
- [55] David G Lowe. Distinctive image features from scale-invariant keypoints. *Intl. Journal of Computer Vision (IJCV)*, 2004.

Appendices

In the appendices, we present more experimental results and analysis to show the effectiveness of DRC-Net. In Appendix A, we provide five alternatives to the FPN-like structure for fusing the dual-resolution feature maps of the feature backbone. In Appendix B, we compare DRC-Net with other neighbourhood consensus based methods in more details. Finally, in Appendix C, we qualitatively compare DRC-Net with the state-of-the-art methods on three benchmarks. DRC-Net establishes the new state-of-the-art. Besides, we also enclose the demo code with pre-trained models. All our code and pre-trained models will be made publicly available.

A Investigation on more variants of FPN structure

Apart from the dual-resolution feature extractor we present in the main paper, we also investigate other possible FPN-like architectures (shown in Figure 8) and thoroughly evaluate their effects on the matching performance.

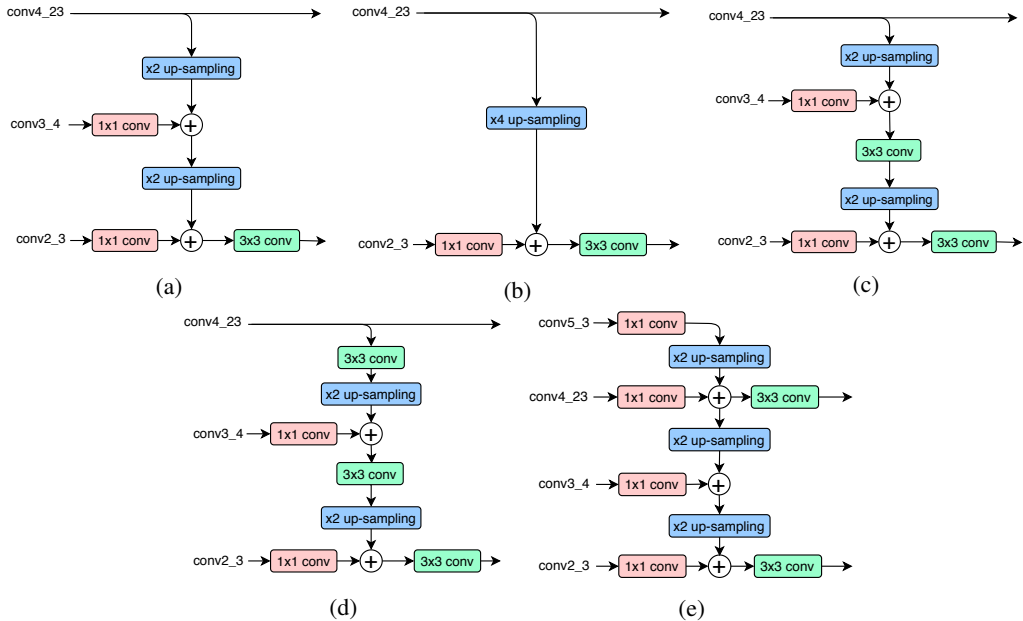


Figure 8: Five variants of FPN architecture. (a) is our default architecture used in the main paper. In (b), we directly fuse the output of conv4_{23} with that of conv2_3 by up-sampling 4 times. In (c) and (d), additional 3×3 conv modules are adopted before up-sampling. In (e), we incorporate the output of conv5_3 . The channels of all feature maps are aligned to 1024 by 1×1 conv layers.

We experiment with different alternatives of the FPN based dual-resolution feature extractor in DRC-Net and evaluate the model on HPatches [23] as well as InLoc [24] benchmarks. The results are reported in Figure 9 and Figure 10 respectively.

As shown in Figure 9, all five types of variants have similar overall performance. Type (b) and Type (e) are slightly inferior on illumination change at small thresholds but all five types have almost identical performance on viewpoint change. Overall, type (d) very slightly outperforms others but at the cost of more parameters in the 3×3 convolutional layers than type (a). Similarly, in Figure 10, we can see the five types of variants also have similar performance on InLoc benchmark. Type (b) is marginally behind others while type (a), (c), (d) and (e) have entangled curves such that no type consistently outperform others. These results reveal that type (b) is marginally inferior than other types as it only contains the information from two layers while the rest of the types have almost the same performance. Therefore, we select type (a) which has, except type (b), the simplest architecture among five options as our dual-resolution feature extractor.

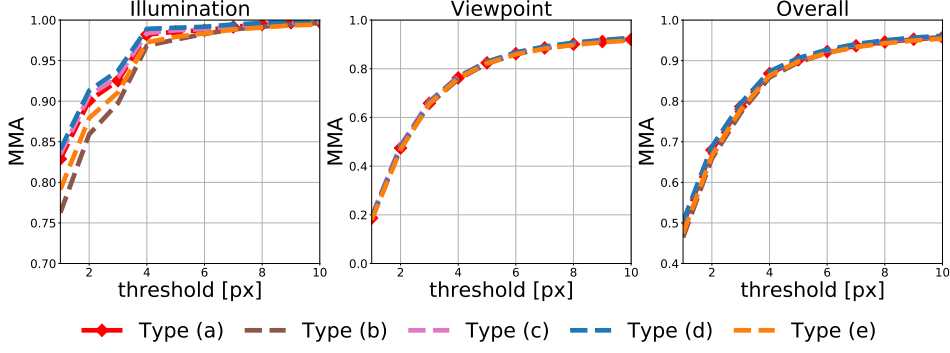


Figure 9: Performance of different variants of FPN architecture on HPatches benchmark. The input image size is 1600×1200 and the top 1000 matches are selected for the evaluation of MMA.

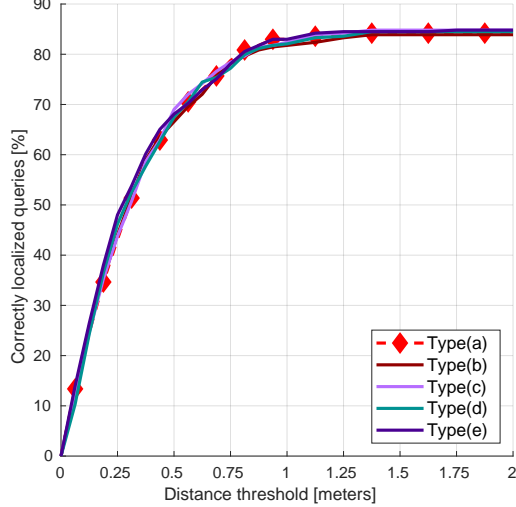


Figure 10: Performance of different variants of FPN architecture on InLoc benchmark. Input images have the image size of 1600×1200 .

Additionally, we also compare type (a) and type (e) with their 256 channel counterparts in Figure 11. Notice that the 256 channel counterpart of type (e) is the original FPN [22]. We can see that increasing number of channels does not affect the performance of type (e). However, type (a) with 1024 channels performs better than that with 256 channels under huge illumination variations at smaller thresholds. This further justifies that type (a) is a more proper choice for DRC-Net.

B Comparison with other neighbourhood consensus based methods

In this section, we compare DRC-Net with Sparse-NCNet [6] and NCNet [5] on HPatches benchmark in more details. In Figure 12a, we show the performance of the three methods given input images with the same size of 1600×1200 . DRC-Net achieves the best results in all cases except under huge illumination changes with a threshold less than 3 pixels. The success attributes to that DRC-Net can generate a larger relocalisation feature map under the same input image size. In Figure 12b, we compare the performance of the three methods with the same relocalisation feature map size of 200×100 . DRC-Net achieves the best performance under huge illumination variations, but it does not perform as well as the other two methods under huge viewpoint variations. Overall, DRC-Net performs on par with both Sparse-NCNet and NCNet. We hypothesise two reasons for the deterioration in huge viewpoint variation. One is that the input image size for DRC-Net is only a half of Sparse-NCNet and a quarter of NCNet hence some valuable information are lost in the down-sampled input image. Second, the 4D correlation tensor of DRC-Net is only $50 \times 38 \times 50 \times 38$

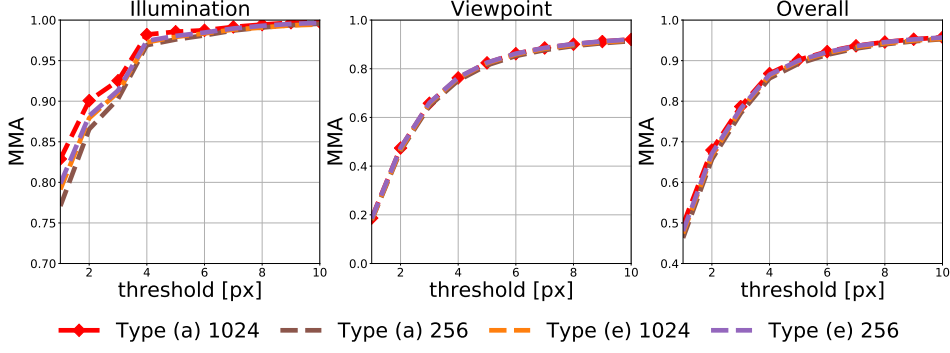
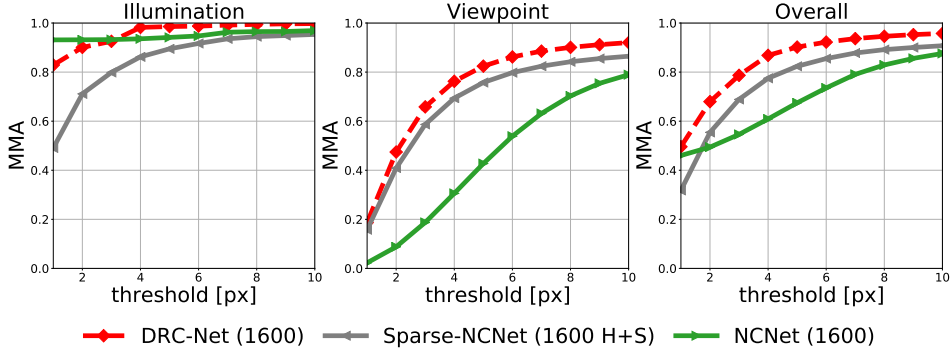


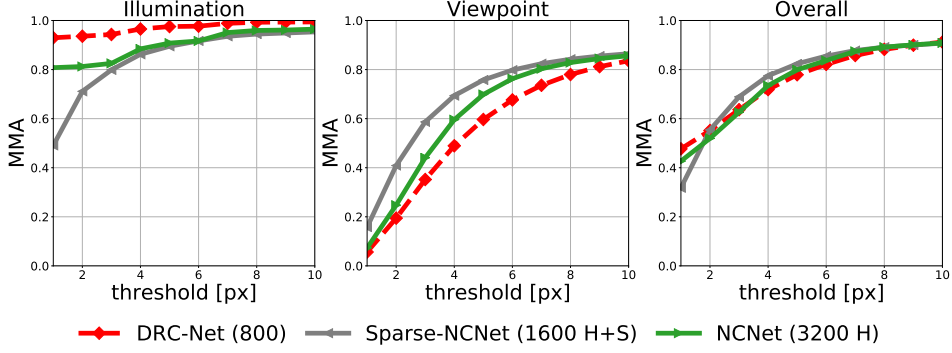
Figure 11: Comparison between 256 and 1024 output feature channels for type (a) and type (e). Notice that type (e) with 256 channels is the original FPN architecture.

while the other two methods have the size of $100 \times 75 \times 100 \times 75$. Smaller 4D correlation tensor indicates weaker filtering effect from the neighbourhood consensus module which could lead to worse performance under huge viewpoint changes. In Figure 12c we demonstrate that DRC-Net can achieve similar or better results on HPatches with a much smaller image size than other methods, which further verifies the effectiveness of our dual-resolution design in DRC-Net.

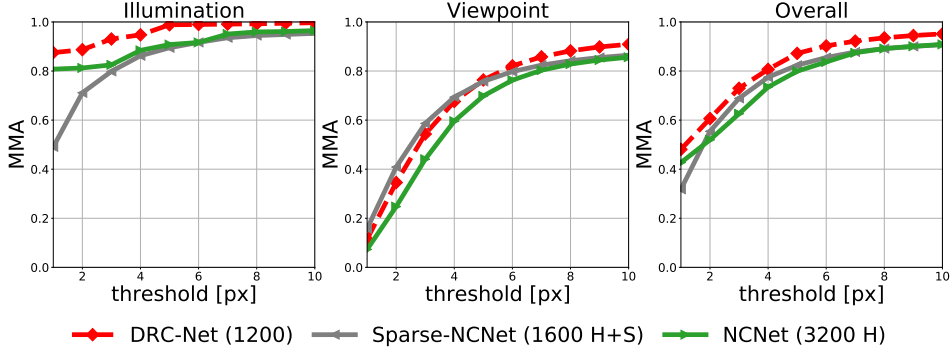
We notice an interesting trend in Figure 12 that a larger relocalisation resolution leads to better performance under illumination changes but worse performance under viewpoint changes at small thresholds. This could be explained as follows. A smaller localisation resolution means that features are more sparsely distributed on the image. Each feature covers a greater image area so that the difference between nearby features is more distinctive. Moreover, as there is no homographic change between the image pair, the correct correspondence of one point in image I^A will be at the same location in image I^B , hence there is no need to search other places. Therefore, feature resolution has little impact on the performance under illumination change. However, under viewpoint changes, the relocalisation feature resolution matters more. If the resolution is small, the model will not be able to capture the viewpoint changes as the features are spatially too coarse compared with the original image. With a larger feature resolution, the discrepancy between nearby locations can be properly captured, therefore, more robust matching can be achieved.



(a) All methods have the same input image size of 1600×1200 . The relocalisation feature resolutions of DRC-Net, Sparse-NCNet and NC-Net are 400×300 , 200×100 and 100×75 respectively.



(b) All methods have the same relocalisation resolution of 200×150 . The input image sizes for DRC-Net, Sparse-NCNet, and NCNet are 800×600 , 1600×1200 and 3200×2400 respectively.



(c) DRC-Net can achieve better results with a smaller input image size. The input image sizes for DRC-Net, Sparse-NCNet and NCNet are 1200×900 , 1600×1200 and 3200×2400 respectively.

Figure 12: Comparing DRC-Net with Sparse-NCNet and NCNet.

C Qualitative comparison

In this section, we provide more qualitative results of DRC-Net on HPatches, InLoc, and Aachen Day-Night benchmarks and compare with Sparse-NCNet and NCNet. The results for Sparse-NCNet and NCNet are obtained using the pre-trained models provided by the authors under the best configurations reported in the original papers. The input image sizes are 1600×1200 for DRC-Net and 3200×2400 for both Sparse-NCNet and NCNet.

HPatches benchmark We qualitatively compare DRC-Net with Sparse-NCNet and NCNet on HPatches benchmark [23]. Top 6000 matches are selected for each method. The correspondences with a re-projection error less than 3 pixels are considered to be correct and are marked as green dots. Otherwise, the correspondences are considered to be wrong and are marked as red dots. We demonstrate that DRC-Net performs notably better than others under challenging illumination variations and performs on par with others under huge viewpoint changes.

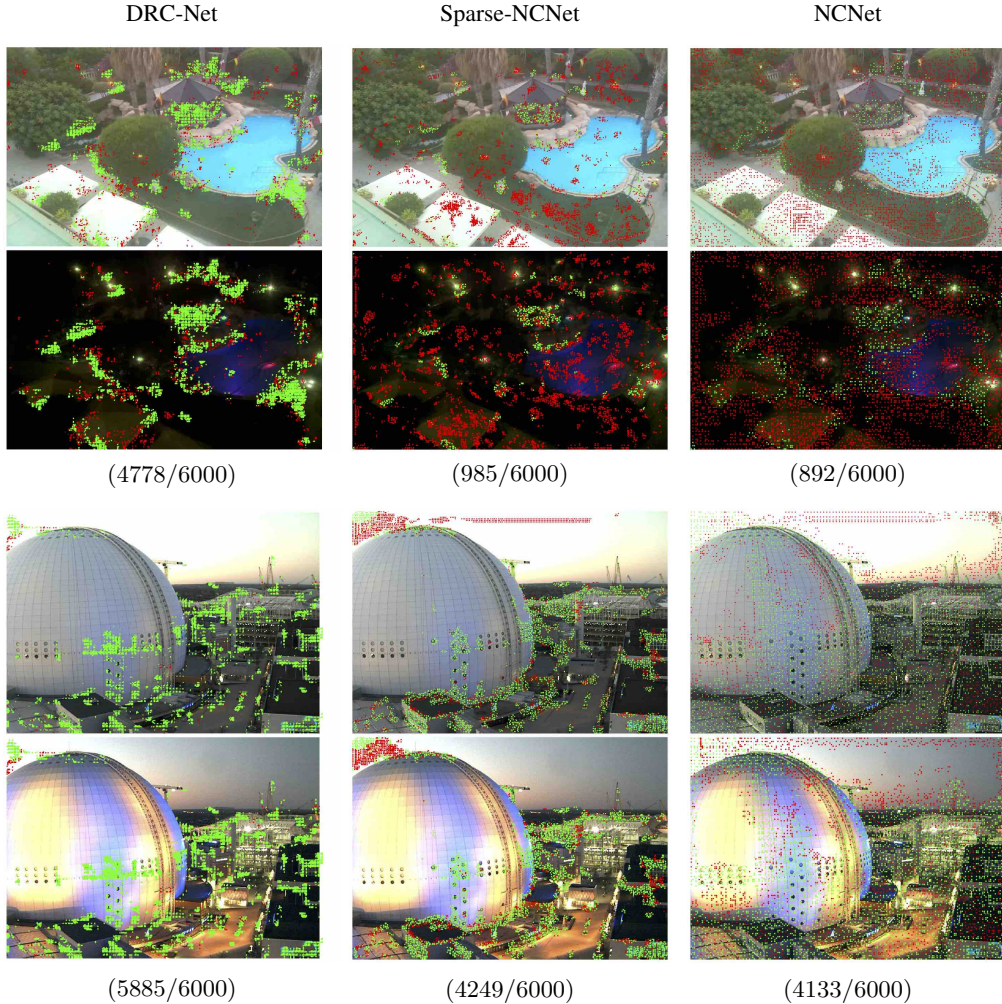


Figure 13: Comparison on HPatches benchmark under huge illumination changes. Top 6000 matches are selected and the threshold is set as 3 pixels. DRC-Net performs the best under challenging illumination variations. We also report (correct/total) matches under each pair.

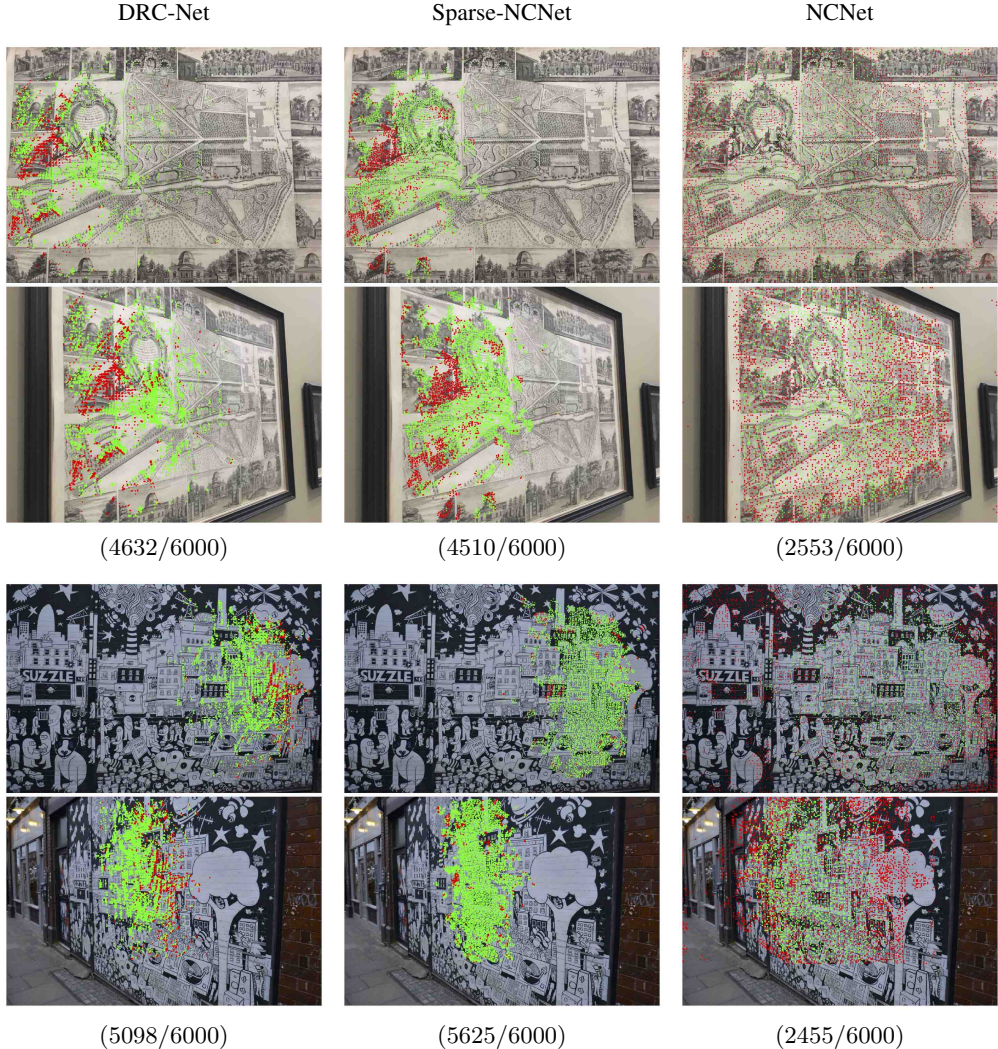


Figure 14: Comparison on HPatches benchmark under huge viewpoint changes. DRC-Net substantially outperforms NCNet and performs on par with Sparse-NCNet. We also report (correct/total) matches under each pair.

InLoc benchmark We qualitatively compare DRC-Net with Sparse-NCNet on InLoc benchmark [24]. Query images were taken a few months after the database images being collected. As no ground truth is provided, we can only assess the quality of correspondences by visual inspection. In Figure 15, we demonstrate that DRC-Net is able to establish reliable correspondences for indoor scenes having very large viewpoint variations, illumination changes and repetitive patterns.

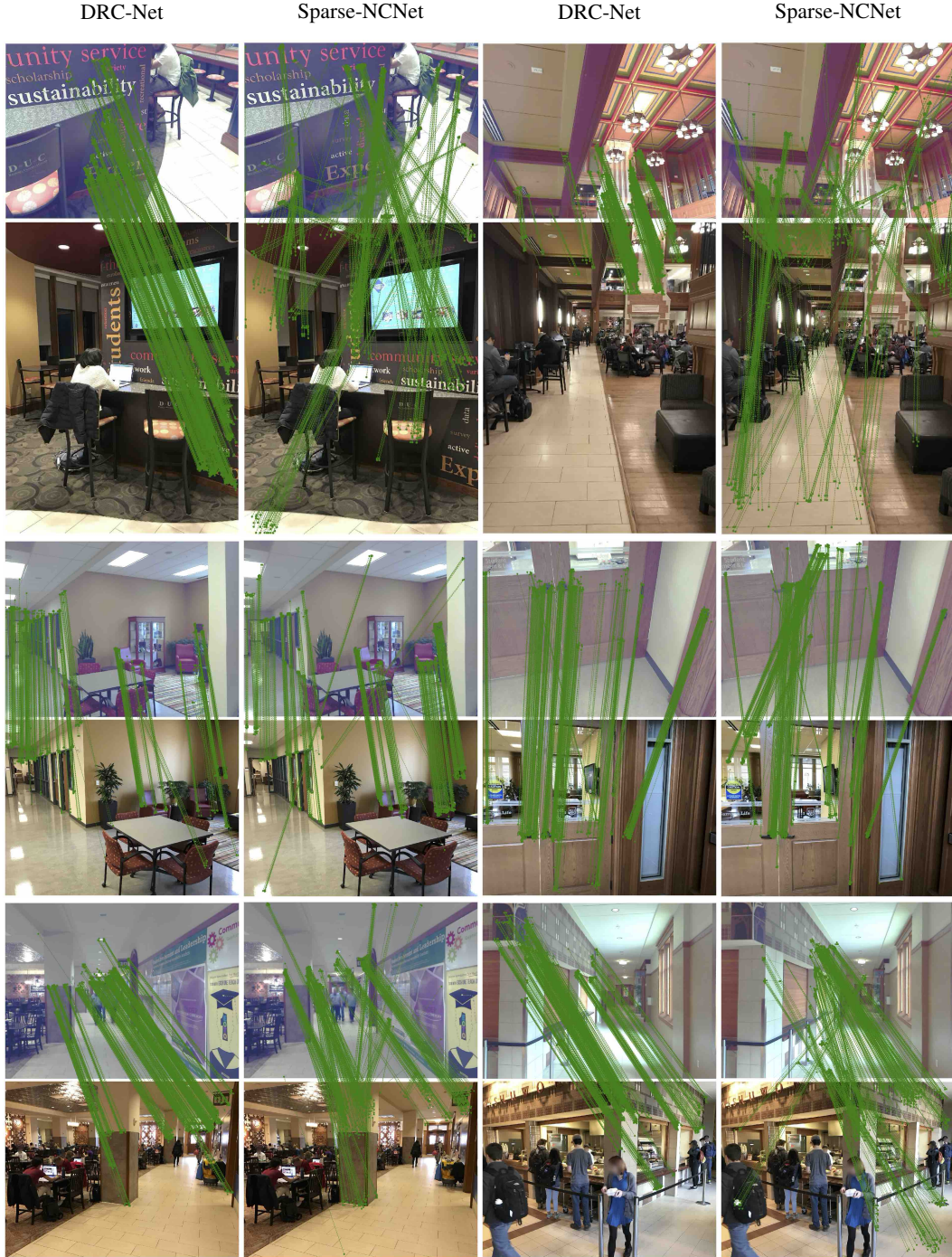


Figure 15: Qualitative comparison on InLoc. Top 500 matches are selected for each method.

Aachen Day-Night benchmark We qualitatively compare DRC-Net with Sparse-NCNet on Aachen Day-Night benchmark [48]. As no ground truth is available, we can only assess the quality of the correspondence by visual inspection. From Figure 16, DRC-Net is able to produce reliable correspondences for outdoor scenes having very large viewpoint changes, day-night illumination changes and repetitive patterns.

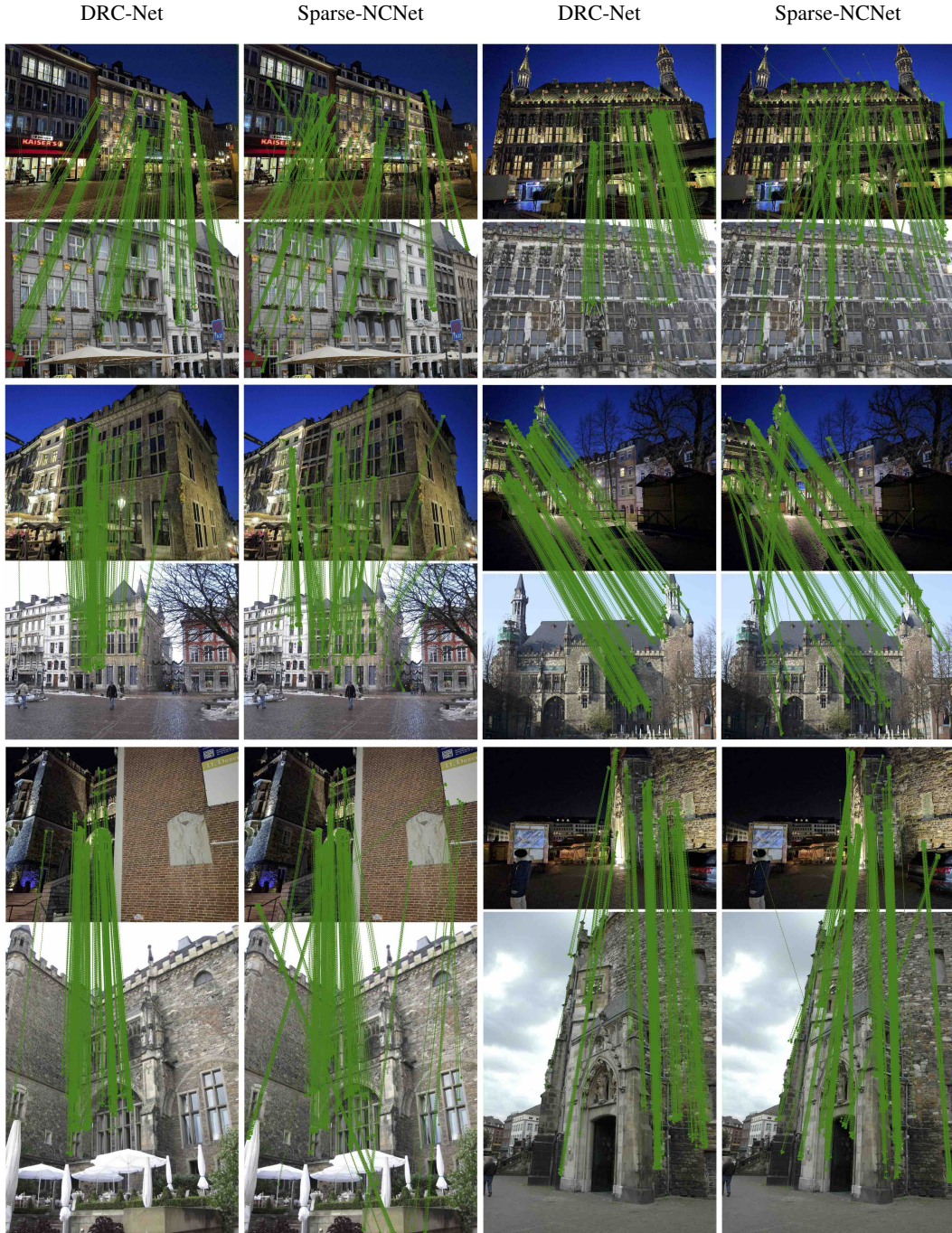


Figure 16: Qualitative comparison on Aachen Day-Night. Top 500 matches are selected for each method.